Dynamics of Macromolecules

R. G. Winkler

This document has been published in

Manuel Angst, Thomas Brückel, Dieter Richter, Reiner Zorn (Eds.):
Scattering Methods for Condensed Matter Research: Towards Novel Applications at Future Sources
Lecture Notes of the 43rd IFF Spring School 2012
Schriften des Forschungszentrums Jülich / Reihe Schlüsseltechnologien / Key Technologies, Vol. 33
JCNS, PGI, ICS, IAS
Forschungszentrum Jülich GmbH, JCNS, PGI, ICS, IAS, 2012
ISBN: 978-3-89336-759-7

B 6 Dynamics of Macromolecules [1]

R. G. Winkler
Institute for Advanced Simulation
Forschungszentrum Jülich GmbH

Contents

[1] Lecture Notes of the 43rd IFF Spring School "Scattering Methods for Condensed Matter Research: Towards Novel Applications at Future Sources" (Forschungszentrum Jülich, 2012).

1 Introduction

Macromolecule, such as linear polymers, are ubiquitous in everyday products and in biological systems. The spectrum of applications of synthetic polymers is wide and covers such divers fields as medicine (heart valves, blood vessels, drug deliver systems), consumer (containers, clothing, fluid modifiers, suspension stabilizer) and industrial products (automobile parts, adhesives, elastomers, tyres, viscosity modifiers) as well as sports equipment (helmets, balls, golf clubs). (The chemical structures of various polymers are introduced in the contribution E 2 of this lecture notes.) Moreover, macromolecules constitute an integral part of biological systems. Proteins, for example, carry the major part of the mechanical and chemical functions of cells. Desoxyribonucleic acid (DNA) is the molecular basis of heredity and is constructed of a double helix. The extraordinary mechanical and dynamical properties of eukaryotic cells are determined by a three dimensional assembly of protein fibers, the cytoskeleton. A major contribution to this remarkable properties is due to actin filaments, which consist of two strands of globular molecules called actin, and proteins that cross-link them [1, 2]. These molecules are often denoted as semiflexible polymers. A key aspect of DNA structure is its large length-to-width ratio. The diameter of the molecule is approximately 2 nm, whereas typical contour lengths range from micrometers in simple viruses to centimeters in humans. Thus, its structural and dynamical properties can easily by analyzed by optical methods. From a theoretical point of view, this makes DNA an ideal candidate to verify polymer models.

To control the behavior of polymers, an understanding of their dynamical behavior is inevitable. On the one hand, such fundamental knowledge helps to improve production processes, e.g., in injection molding, or to modify the viscoelastic behavior of solutions. On the other hand, by measurements of the polymer dynamics via, e.g., neutron scattering or nuclear magnetic resonance (NMR), insight is gained into the structural properties of polymers and their environment.

Polymers constitute a unique class of material. Thermodynamically, the free energy of condensed matter is given by the Helmholtz free energy $A = E - TS$, where E is the internal energy, T the absolute temperature, and S is the entropy [3–8]. In solids, the internal energy (phonons) dominates over the the entropic part. In contrast, the free energy of polymers is determined by the entropy [9–16]. This implies that other concepts have to be devised to describe the structural and dynamical properties of polymers. Solids often form crystalline lattices, with well-defined equilibrium positions, around which the atoms perform oscillatory motions. In contrast, flexible and semiflexible polymers are able to undergo a huge spectrum of conformational changes at a constant energy. This is illustrated in Fig. 1, where various possible conformations are shown of DNA fragments.

To cope with the huge number of internal degrees of freedom of polymers, their properties are described by statistical physics [9–16]. Here, no longer an individual system is considered, but rather an ensemble of identical systems possessing the same macroscopic properties, e.g., the same number of particles, volume, and mean energy. This provides a distribution function, or a probability density, for their possible conformational states [14, 16]. For the description of the polymer dynamics, stochastic methods are exploited. Here, an effective single polymer approach is adopted, where the influence of the surrounding is taken into account by a stochastic process. In the simplest case, the environment is described by a white-noise random process, i.e., a Gaussian and Markovian process [17, 18]; this applies approximately to polymer melts.

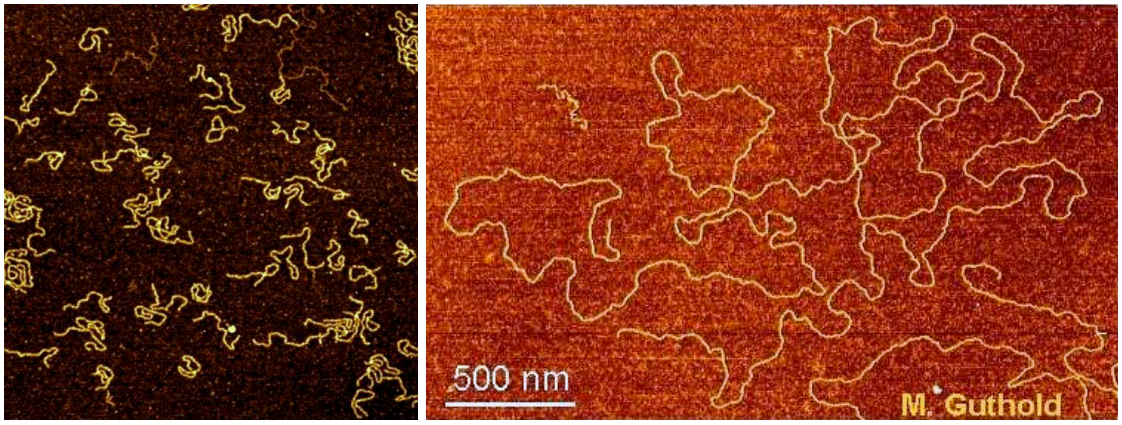

Fig. 1: *AFM images of DNA molecules adsorbed and immobilized on a solid substrate. Short fragments of DNA (left); images size* $1\mu\mathrm{m} \times 1\mu\mathrm{m}$. *Lambda DNA (right), a rather flexible molecule, is composed of 48 502 bp (base pairs), which approximately corresponds a contour length of* $L = 16.49$ *µm. Images are taken from* http://www.dmphotonics.com/AFM-STM-NSOM-sample-quotes/Sample%20quotes%20for%20AFM-STM-NSOM%20Heron.htm *(left) and* http://www.wfu.edu/ gutholdm/research.html *(right).*

For polymers in solution, hydrodynamic interactions between monomers have to be taken into account [14, 19, 20], which are mediated by fluid flow. In melts of very long polymers, the non-crossability of polymers plays a major role and gives rise to dynamical restrictions by neighboring polymers, denoted as entanglements [14]. The polymer dynamics is then described by the reptation model [11, 14, 21, 22].

2 Gaussian Polymer

There are suitable all-atom models for polymers, which are exploited in computer simulations. However, typically only simple, low molecular weight polymers are considered, e.g., alkane molecules. Instead, coarse-grained polymer models are used to study properties of long macromolecules, in particular in analytical theory.

The generic features of a polymer—its conformational degrees of freedom—can be described and captured by a Gaussian model. Typically, this model yields the correct qualitative properties of flexible and semiflexible polymers, often it is even quantitatively correct [14,23–26]. In such a model, details of the bonds are neglected, even several monomers are combined in an effective segment, merely the connection matters into a linear structure. Denoting the connecting vector between two successive "monomers" along the polymer chain by $\boldsymbol{R}_i = \boldsymbol{r}_i - \boldsymbol{r}_{i-1}$ $(i = 1, \ldots, N)$ (cf. Fig. 2), the Gaussian chain is characterized by the first two moments, namely $\langle \boldsymbol{R}_i \rangle = 0$, i.e., all orientations are equally probable, and $\langle \boldsymbol{R}_i^2 \rangle = l^2$, where $\langle \ldots \rangle$ denotes the ensemble average, at equilibrium. All higher moments can be expressed by these two moments [17]. Considering the non-zero second moment as a constraint, the (configurational) distribution function $\Psi(\{\boldsymbol{r}\})$ and partition function Z can be obtained by the maximum entropy principle, which provides a basis for the systematic derivation of distribution function also in the presence of external fields and bending stiffness [16, 24, 26–28]. The distribution and partition functions for all monomers

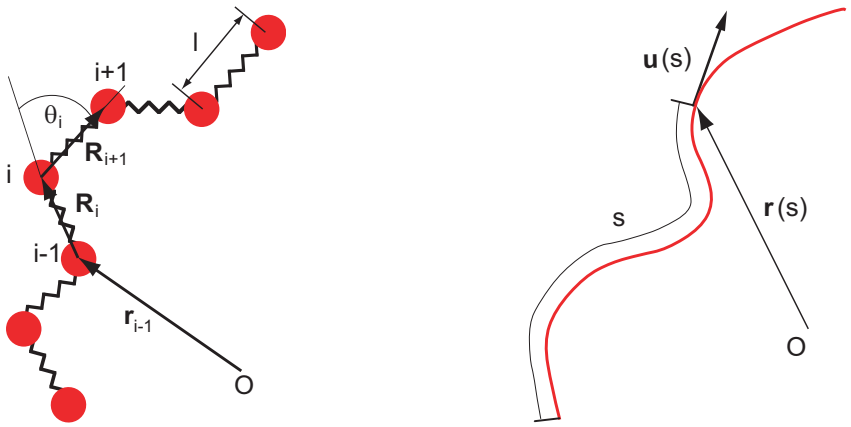

Fig. 2: *Models of a discrete (left) and a continuous (right) linear polymer. The tangent vector* $\boldsymbol{u}(s) = \partial \boldsymbol{r}(s)/\partial s$ *is obtained in the limit* $\boldsymbol{R}_i/l \to \boldsymbol{u}(s)$, $il \to s$ *for* $l \to 0$.

are given by the Gaussian

$$\Psi(\{\boldsymbol{r}\}) = \frac{1}{Z} \exp\left(-\frac{3}{2l^2}\sum_{i=1}^{N} \boldsymbol{R}_i^2\right), \tag{1}$$

$$Z = \int \exp\left(-\frac{3}{2l^2}\sum_{i=1}^{N} \boldsymbol{R}_i^2\right) d^{3N}R, \tag{2}$$

where $\boldsymbol{r}_0 = 0$ is used to remove the translation degree of freedom. Note that the total partition function $Z_{tot} = ZZ_k$ is the product of the configurational part (2) and the contribution by the kinetic energy $Z_k = (2\pi m k_B T)^{3N/2}$ ($\boldsymbol{v}_0 = 0$), where m is the mass of a monomer. Equation (1) and (2) are reminiscent of a system of independent harmonic oscillators with the potential energy $V_i = 3k_BT\boldsymbol{R}_i^2/(2l^2)$. From the point of view of the underlying physics, however, the equations capture the conformational degrees of freedom of a polymer rather then energetic aspects. The Gaussian polymer is self-similar, as the distribution of segment lengths is similar to the end-to-end vector distribution function

$$\Psi(\boldsymbol{r}_N) = \left(\frac{3}{2\pi N l^2}\right) \exp\left(-\frac{3}{2Nl^2}\boldsymbol{r}_N^2\right), \tag{3}$$

with the mean square end-to-end distance $\langle(\boldsymbol{r}_N - \boldsymbol{r}_0)^2\rangle = Nl^2$. The maximum entropy principle yields the conformational entropy [16, 28]

$$S = k_B \ln Z + \frac{3}{2} N k_B, \tag{4}$$

where the last term accounts for the potential energy of the bonds.

For various calculations, a continuous polymer model is advantageous. From a physical point of few, it does not matter whether a continuous or discrete model is used. Because of the adopted abstraction of a real polymer, the chosen description applies on large length scales only. For a Gaussian polymer model, only properties are described on the length scale larger than the segment length l.

The continuum limit $N \to \infty$, $l \to 0$, such that $L = Nl = const.$, where L is the contour length of the polymer, yields

$$Z = \int \exp\left(-\sum_{i=1}^{N} \frac{3}{2l^2}\boldsymbol{R}_i^2\right) d^{3N}r \overset{l\to 0, N\to\infty}{\longrightarrow} \int \exp\left(-\frac{3}{2l}\int_0^L \left(\frac{\partial \boldsymbol{r}}{\partial s}\right)^2 ds\right) \mathcal{D}^3 r,$$

i.e., a functional integral (path integral) is obtained. However, in the limit $l \to 0$, $3/(2l) \to \infty$ and the partition function approaches zero ($\lim_{l\to 0} Z = 0$), i.e., the polymer collapses into a point. The reason is that the distribution function (1) corresponds to a Wiener process [17], and the derivative of the 'trajectory', i.e., the polymer contour, does not exist. A meaningful continuum limit can only be performed for a semiflexible polymer [16, 24]. For the Gaussian polymer, a continuum description can only be adopted on length scales $s \gg l$. Hence, the length l is assumed to be small, but finite and the partition function reads

$$Z = \int \exp\left(-\frac{3}{2l}\int_0^L \left(\frac{\partial \boldsymbol{r}}{\partial s}\right)^2 ds\right) \mathcal{D}^3 r. \tag{5}$$

l is sometimes denoted as Kuhn length l_K and is related to the polymer persistence length l_p via $l_K = l = 2l_p$.
The distribution function of two points $\boldsymbol{r}(s)$, $\boldsymbol{r}(s')$, with $\Delta\boldsymbol{r} = \boldsymbol{r}(s) - \boldsymbol{r}(s')$, is

$$\Psi(\Delta\boldsymbol{r}) = \left(\frac{3}{2\pi\sigma^2(s,s')}\right)^{3/2} \exp\left(-\frac{3\Delta\boldsymbol{r}^2}{2\sigma^2(s,s')}\right), \tag{6}$$

where $\sigma^2(s,s') = \left\langle \left(\boldsymbol{r}(s) - \boldsymbol{r}(s')\right)^2 \right\rangle = l|s-s'|$. The radius of gyration is obtained as $R_G^2 = lL/6$.

In order to describe the properties of semiflexible polymers such as DNA or actin filaments, specifically their resistance to bending, a bending energy has to be taken into account. Kratky and Porod suggested an energy, which is determined by the square of the local curvature of the continuous polymer model [29]

$$\frac{V_B}{k_B T} = \frac{\epsilon_p}{2}\int_0^L \frac{1}{R(s)^2} ds = \frac{\epsilon_p}{2}\int_0^L \left(\frac{\partial^2 \boldsymbol{r}(s)}{\partial s^2}\right)^2 ds. \tag{7}$$

Taking bending restrictions into account, the partition function of a Gaussian semiflexible polymer is [16, 20, 23–27, 30]

$$Z = \int \exp\left(-\frac{3}{4l_p}\int_0^L \left(\frac{\partial \boldsymbol{r}(s)}{\partial s}\right)^2 ds - \frac{3}{4}\left[\left(\frac{\partial \boldsymbol{r}(0)}{\partial s}\right)^2 + \left(\frac{\partial \boldsymbol{r}(L)}{\partial s}\right)^2\right] - \frac{3l_p}{4}\int_0^L \left(\frac{\partial^2 \boldsymbol{r}(s)}{\partial s^2}\right)^2 ds\right) \mathcal{D}^3 r\,. \tag{8}$$

Since this is a Gaussian function, Eq. (6) applies with

$$\sigma^2(s,s') = 2l_p|s-s'| - 2l_p^2\left(1 - e^{-|s-s'|/l_p}\right). \tag{9}$$

This equation reduces to the expression $\sigma^2 = 2l_p|s-s'|$ for $L/l_p \gg |s-s'|/l_p \gg 1$, i.e., flexible polymer behavior, and $\sigma^2 = (s-s')^2$ for $|s-s'|/l_p \ll 1$, which corresponds to (local) rodlike behavior. In the case $L/l_p \ll 1$, the latter applies to all distances $|s-s'|$.

3 Dynamics of Flexible Polymers

The dynamics of a polymer is determined by its interactions with the environment. For a polymer in a melt, i.e., in a dense environment of similar polymers, the local frictional interactions dominate. In contrast, the dynamics of a polymer in dilute solution is determined by fluid mediated interactions. Here, the motion of a monomer implies fluid motion due to no-slip boundary conditions, i.e., locally the fluid at the position of a particle moves with the same velocity as the particle itself and vice versa. This fluid motion affects the dynamics of other particles and is denoted as hydrodynamic interactions [14, 19]. Aside from that, intramolecular forces are present. In the continuum limit, the "potential energy"

$$V = \frac{3k_BT}{2l}\int_0^L \left(\frac{\partial \boldsymbol{r}(s)}{\partial s}\right)^2 ds \tag{10}$$

yields the local force

$$\boldsymbol{F}(s) = \frac{3k_BT}{l}\frac{\partial^2 \boldsymbol{r}(s)}{\partial s^2} \tag{11}$$

on the point $\boldsymbol{r}$ at s along the polymer contour. Note, all points of the polymer are free.

In the following, only the limit $L/l \gg 1$ will be considered, i.e., only the dynamics of flexible polymers will be addressed in detail. The dynamics of semiflexible polymers is discussed in Refs. [20, 23, 25–27].

3.1 Free-Draining Dynamics—Rouse Model

The friction-dominated dynamics, i.e., no hydrodynamic interactions, is denoted as free-draining dynamics (Rouse model [14, 31]). Here, the equation of motion of the point $\boldsymbol{r}(s,t)$ is given by

$$\gamma\frac{\partial \boldsymbol{r}(s,t)}{\partial t} = \frac{3k_BT}{l}\frac{\partial^2 \boldsymbol{r}(s,t)}{\partial s^2} + \boldsymbol{\Gamma}(s,t), \tag{12}$$

with the friction constant γ and the stochastic force $\boldsymbol{\Gamma}(s,t)$. Since a polymer is long and hence its dynamics is slow compared to fluctuations in the environment, the over-damped equation is considered only, i.e., inertia effects are neglected—their influence on the dynamics has decayed on the polymer-relevant time scales (see also contribution B3) [14, 19]. The equation of motion is complemented by the boundary conditions

$$\left.\frac{\partial \boldsymbol{r}(s,t)}{\partial s}\right|_{s=0,L} = 0 \tag{13}$$

and the correlation functions of the stochastic force, which is assumed to be Gaussian and Markovian (white noise),

$$\langle \boldsymbol{\Gamma}(s,t)\rangle = 0\ , \tag{14}$$

$$\langle \Gamma_\alpha(s,t)\Gamma_{\alpha'}(s',t')\rangle = 2\gamma k_BT\delta_{\alpha\alpha'}\delta(t-t')\delta(s-s')\ . \tag{15}$$

Equation (12) is a linear partial differential equation, which is easily solved by an eigenfunction expansion. The relevant eigenvalue equation is

$$\frac{3k_BT}{l}\frac{\partial^2}{\partial s^2}\varphi_n(s) + \xi_n\varphi_n = 0\ , \tag{16}$$

with the eigenfunctions φ_n and the eigenvalues ξ_n. With the boundary conditions $\partial\varphi_n/\partial s = 0$ at $s = 0, L$ follows

$$\varphi_0 = \sqrt{\frac{1}{L}}\,, \qquad \xi_0 = 0\,, \tag{17}$$

$$\varphi_n = \sqrt{\frac{2}{L}}\cos\frac{n\pi s}{L}\,, \qquad \xi_n = \frac{3\pi^2 k_B T n^2}{lL^2} \quad \forall\, n > 0\,. \tag{18}$$

With the eigenfunction expansion

$$\boldsymbol{r}(s,t) = \sum_{n=0}^{\infty} \boldsymbol{\chi}_n(t)\varphi_n(s)\,, \qquad \boldsymbol{\Gamma}(s,t) = \sum_{n=0}^{\infty} \boldsymbol{\Gamma}_n(t)\varphi_n(s), \tag{19}$$

Eq. (12) yields the Langevin equations

$$\frac{d}{dt}\boldsymbol{\chi}_0 = \frac{1}{\gamma}\boldsymbol{\Gamma}_0\,; \qquad \frac{d}{dt}\boldsymbol{\chi}_n = -\frac{1}{\tau_n}\boldsymbol{\chi}_n + \frac{1}{\gamma}\boldsymbol{\Gamma}_n\,,\ n > 0\,, \tag{20}$$

for the normal-mode amplitudes $\boldsymbol{\chi}_n$, with the relaxation times

$$\tau_n = \frac{\gamma}{\xi_n} = \frac{\gamma l L^2}{3\pi^2 k_B T n^2} \equiv \frac{\tau_R}{n^2}\,, \quad \forall n > 0, \tag{21}$$

and the correlations $\left\langle \Gamma_n^{\alpha}(t)\Gamma_m^{\alpha'}(t')\right\rangle = 2\gamma k_B T\delta_{\alpha\alpha'}\delta_{nm}\delta(t-t')$. $\tau_R = \gamma l L^2/(3\pi^2 k_B T)$ is the Rouse relaxation time [14]. It is important to note that the relaxation times exhibit a quadratic length and mode-number dependence. The solution of the Langevin equation (20) (Ornstein-Uhlenbeck process) is [17]

$$\boldsymbol{\chi}_0(t) = \boldsymbol{\chi}_0(0) + \frac{1}{\gamma}\int_0^t \boldsymbol{\Gamma}_0(t')\,dt'\,; \qquad \boldsymbol{\chi}_n(t) = \frac{1}{\gamma}\int_{-\infty}^t \exp\left(-\frac{t-t'}{\tau_n}\right)\boldsymbol{\Gamma}_n(t')\,dt'\,. \tag{22}$$

Hence, the solution of Eq. (12) is given by

$$\boldsymbol{r}(s,t) = \boldsymbol{\chi}_0(t)\varphi_0 + \sum_{n=1}^{\infty}\frac{1}{\gamma}\int_{-\infty}^t \exp\left(-\frac{t-t'}{\tau_n}\right)\boldsymbol{\Gamma}_n(t')dt'\varphi_n(s). \tag{23}$$

With that expression, various dynamical properties of polymers can be calculated.

(i) **Center-of-mass mean square displacement**

The center-of-mass of a polymer is defined as

$$\boldsymbol{r}_{cm}(t) = \frac{1}{L}\int_0^L \boldsymbol{r}(s,t)\,ds = \boldsymbol{\chi}_0(t)\varphi_0. \tag{24}$$

Hence, its mean square displacement (MSD) is

$$\left\langle \Delta\boldsymbol{r}_{cm}(t)^2\right\rangle = \frac{1}{L}\left\langle(\boldsymbol{\chi}_0(t) - \boldsymbol{\chi}_0(0))^2\right\rangle = \frac{1}{\gamma^2 L}\int_0^t\int_0^t \langle\boldsymbol{\Gamma}_0(t')\boldsymbol{\Gamma}_0(t'')\rangle\,dt'dt'' = \frac{6k_BT}{\gamma L}t, \tag{25}$$

or $\left\langle \Delta\boldsymbol{r}_{cm}(t)^2\right\rangle = \left\langle(\boldsymbol{r}_{cm}(t) - \boldsymbol{r}_{cm}(0))^2\right\rangle = 6D_R t$, where $D_R = k_BT/(\gamma L)$ is the center-of-mass diffusion coefficient, which inversely proportional to the polymer length.

(ii) **Segmental mean square displacement**

The mean square displacement of the point $\boldsymbol{r}(s,t)$ is given by

$$\left\langle \Delta\boldsymbol{r}(s,t)^2 \right\rangle = \left\langle [\boldsymbol{r}(s,t)-\boldsymbol{r}(s,0)]^2 \right\rangle = \left\langle \Delta\boldsymbol{r}_{cm}(t)^2 \right\rangle + \sum_{n=1}^{\infty} 2\varphi_n(s)^2 \left\langle \boldsymbol{\chi}_n^2 \right\rangle \left(1-e^{-t/\tau_n}\right).$$

With the correlation functions ($n,m>0$)

$$\begin{aligned}\langle \boldsymbol{\chi}_n(t)\boldsymbol{\chi}_m(0)\rangle &= \frac{1}{\gamma^2}\int_{-\infty}^{t}\int_{-\infty}^{0} \exp\left(-\frac{t-t'}{\tau_n}\right)\exp\left(\frac{t''}{\tau_m}\right)\langle \boldsymbol{\Gamma}_n(t')\boldsymbol{\Gamma}_m(t'')\rangle\, dt'dt'' \qquad (26)\\ &= \frac{6k_BT}{\gamma}\delta_{nm}e^{-t/\tau_n}\int_{-\infty}^{0} e^{2t'/\tau_n}dt' = \frac{3k_BT}{\gamma}\tau_n\delta_{nm}e^{-t/\tau_n} = \left\langle \boldsymbol{\chi}_n^2\right\rangle \delta_{nm}e^{-t/\tau_n}\end{aligned}$$

follows

$$\left\langle \Delta\boldsymbol{r}(s,t)^2 \right\rangle = \left\langle \Delta\boldsymbol{r}_{cm}(t)^2 \right\rangle + \frac{6k_BT}{\gamma}\sum_{n=1}^{\infty}\varphi_n(s)^2\tau_n\left(1-e^{-t/\tau_n}\right). \qquad (27)$$

For $t/\tau_R \gg 1$, the second term is a constant, because $e^{-t/\tau_n} \ll 1, \forall n>0$. Since $\langle \Delta\boldsymbol{r}_{cm}(t)^2\rangle \sim t$, the segmental MSD is equal to the center-of-mass MSD in the long-time limit. However, for times $t/\tau_R \ll 1$, the sum is dominated by large mode-number contributions. Then, the MSDs of the various parts of the polymer are different. For example, the center of the polymer ($s=L/2$) moves by a factor of two slower than the ends ($s=0,L$). Averaging over the polymer contour: $\langle \Delta\boldsymbol{r}(t)^2\rangle = \int \langle \Delta\boldsymbol{r}(s,t)^2\rangle\, ds/L$, yields

$$\left\langle \Delta\boldsymbol{r}(t)^2 \right\rangle = \left\langle \Delta\boldsymbol{r}_{cm}(t)^2 \right\rangle + \frac{6k_BT}{\gamma L}\sum_{n=1}^{\infty}\tau_n\left(1-e^{-t/\tau_n}\right). \qquad (28)$$

For $t/\tau_R \ll 1$, the difference between $x_{n+1}=(n+1)\sqrt{t/\tau_R}$ and $x_n = n\sqrt{t/\tau_R}$ is very small and the sum can be replaced by an integral over $x_n = n\sqrt{t/\tau_R}$, i.e.,

$$\begin{aligned}\sum_{n=1}^{\infty}\frac{\tau_R}{n^2}\left[1-e^{-tn^2/\tau_R}\right] &= \sqrt{t\tau_R}\sum_{n=1}^{\infty}\frac{\tau_R}{n^2t}\left[1-e^{-tn^2/\tau_R}\right]\Delta n\sqrt{\frac{t}{\tau_R}}\\ &\longrightarrow \sqrt{t\tau_R}\int_0^{\infty}\frac{1}{x^2}(1-e^{-x^2})dx = \sqrt{t\tau_R}\sqrt{\pi}.\end{aligned}$$

Hence,

$$\left\langle \Delta\boldsymbol{r}(t)^2 \right\rangle = \left\langle \Delta\boldsymbol{r}_{cm}(t)^2 \right\rangle + \frac{6k_BT}{\gamma L}\sqrt{\pi t\tau_R} \overset{t/\tau_R\ll 1}{\longrightarrow} \frac{2lL}{\sqrt{\pi^3}}\sqrt{\frac{t}{\tau_R}}, \qquad (29)$$

i.e. the segments display an anomalous (fractal) diffusion behavior.
The center-of-mass (25) and segmental (28) mean square displacement are displayed in Fig. 3. For $t/\tau_R \ll 1$, the total MSD is dominated by the internal dynamics, i.e., the second term in Eq. (28). As is indicated by the agreement between the full numerical result and the analytical approximation, in that time regime the MSD increase as $t^{1/2}$. For $t/\tau_R \gg 1$, the MSD is given by the center-of-mass displacement.

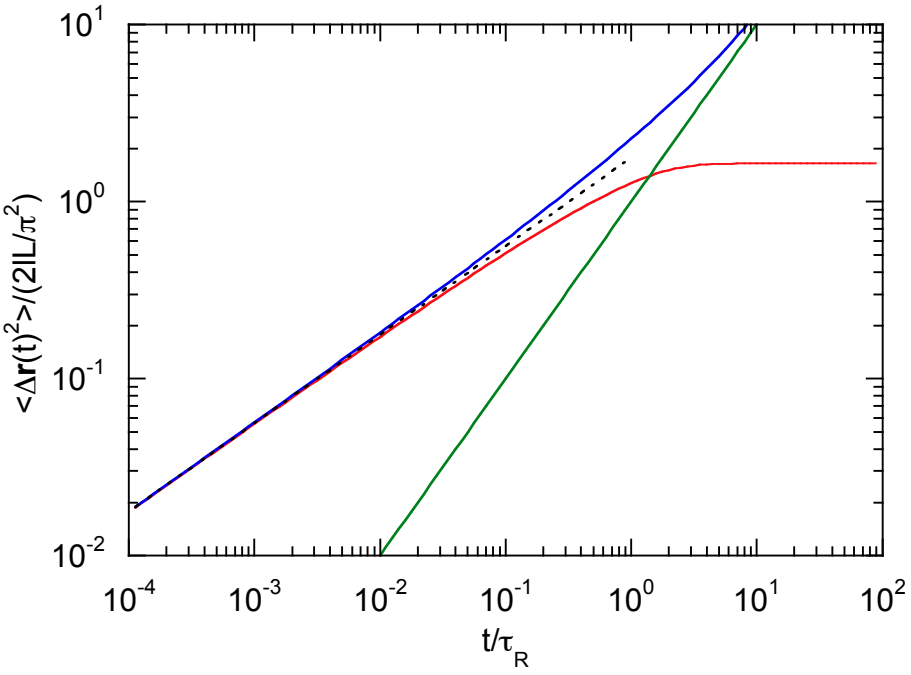

Fig. 3: *Mean square displacements of a free-draining polymer. The green line indicates* $\langle \Delta \boldsymbol{r}_{cm}(t)^2 \rangle$*, the blue line the total MSD* $\langle \Delta \boldsymbol{r}(t)^2 \rangle$*, and the red line the segmental MSD in the center-of-mass reference frame:* $\langle \Delta \boldsymbol{r}(t)^2 \rangle - \langle \Delta \boldsymbol{r}_{cm}(t)^2 \rangle$*. The red line approaches the asymptotic value* $2R_G^2$ *in the limit* $t \to \infty$*. The dotted line represents the analytical approximation (29).*

3.2 Non-Draining Dynamics—Zimm Model

In dilute solution, the polymer dynamics is governed by hydrodynamic interactions. To determine the velocity of a particle at $\boldsymbol{r}(s)$, the fluid velocity field $\boldsymbol{v}(\boldsymbol{r})$ is needed at that position. Since the polymer motion is intimately coupled to the motion of the background fluid, aside from the dynamical equation of the polymer, a dynamical equation for the fluid is needed. To tackle this problem analytically, the fluid is considered a continuum and its dynamics obeys the Navier-Stokes equation or, more precisely, the Stokes equation, since the low Reynolds number limit is considered [14, 19]. As solution of the Stokes equation in response to a volume force $\boldsymbol{f}$, the velocity field is obtained

$$\boldsymbol{v}(\boldsymbol{r}) = \int \boldsymbol{\Omega}(\boldsymbol{r} - \boldsymbol{r}') \boldsymbol{f}(\boldsymbol{r}') \, d^3 r', \tag{30}$$

with the *Oseen* tensor

$$\boldsymbol{\Omega}(\boldsymbol{r}) = \frac{1}{8\pi\eta r} \left(\mathbf{I} + \frac{\boldsymbol{r} : \boldsymbol{r}}{r^2} \right) , \tag{31}$$

where η is the solvent viscosity. A detailed derivation is provide in Appendix A. The Oseen tensor decays like $1/r$. Hence, hydrodynamic interactions are of long-range nature and cannot be neglected. For the continuous polymer chain, the force density is

$$\boldsymbol{f}(\boldsymbol{r}) = \int \left[\boldsymbol{F}(s) + \boldsymbol{\Gamma}(s) \right] \delta(\boldsymbol{r} - \boldsymbol{r}(s)) \, ds, \tag{32}$$

thus,

$$\boldsymbol{v}(\boldsymbol{r}) = \int \boldsymbol{\Omega}(\boldsymbol{r} - \boldsymbol{r}(s)) \left[\boldsymbol{F}(s) + \boldsymbol{\Gamma}(s)\right] ds. \tag{33}$$

In the presence of a solvent, the friction between a particle at $\boldsymbol{r}(s)$ and the fluid background is described by

$$\gamma \left[\dot{\boldsymbol{r}}(s,t) - \boldsymbol{v}(\boldsymbol{r}(s,t))\right] = \boldsymbol{F}(s,t) + \boldsymbol{\Gamma}(s,t). \tag{34}$$

For a particle instantaneously following the fluid flow field $\dot{\boldsymbol{r}}(s,t) = \boldsymbol{v}(\boldsymbol{r}(s,t))$ ($\gamma \to \infty$). In case of a finite slip

$$\dot{\boldsymbol{r}}(s,t) = \boldsymbol{v}(\boldsymbol{r}(s,t)) + \frac{1}{\gamma}\left[\boldsymbol{F}(s,t) + \boldsymbol{\Gamma}(s,t)\right],$$

and the equation of motion of the polymer becomes with Eqs. (11), (33)

$$\frac{\partial \boldsymbol{r}(s,t)}{\partial t} = \int_0^L \mathbf{H}(\boldsymbol{r}(s) - \boldsymbol{r}(s')) \left[\frac{3k_BT}{l}\frac{\partial^2 \boldsymbol{r}(s',t)}{\partial s'^2} + \boldsymbol{\Gamma}(s',t)\right] ds', \tag{35}$$

where the hydrodynamic tensor $\mathbf{H}(\boldsymbol{r}(s))$ is defined as

$$\mathbf{H}(\boldsymbol{r}(s) - \boldsymbol{r}(s')) = \frac{\delta(s-s')}{\gamma}\mathbf{I} + \boldsymbol{\Omega}(\boldsymbol{r}(s) - \boldsymbol{r}(s')). \tag{36}$$

Hydrodynamic interactions control the dynamics of the polymer in solution, however, the polymer conformational properties are not affected. The way conformational space is sampled is different for a non-draining and a free-draining polymer, but not the conformational space itself, at least at equilibrium. This can easily be shown by the stationary state solution of the Fokker-Planck equation corresponding to the Langevin equation (35).

Equation (35) is non-linear and therefore difficult to solve. Thus, for flexible polymers typically the preaveraging approximation is adopted, as originally proposed by Zimm [14, 32]. Here, the hydrodynamic tensor is replaced by its spatially averaged expression $\boldsymbol{\Omega}(\boldsymbol{r}(s) - \boldsymbol{r}(s')) \longrightarrow \langle\boldsymbol{\Omega}(\boldsymbol{r}(s) - \boldsymbol{r}(s'))\rangle$. Utilizing the Gaussian joint probability density (6), the Oseen tensor becomes

$$\langle\boldsymbol{\Omega}(\boldsymbol{r}(s) - \boldsymbol{r}(s'))\rangle = \frac{\mathbf{I}}{6\pi\eta}\left\langle\frac{1}{|\boldsymbol{r}(s) - \boldsymbol{r}(s')|}\right\rangle = \frac{\mathbf{I}}{3\pi\eta}\sqrt{\frac{3}{2\pi l|s-s'|}} \equiv \Omega(s-s')\mathbf{I}. \tag{37}$$

This expression is isotropic, because any non-diagonal part of $\boldsymbol{\Omega}$ vanishes (space is homogeneous and isotropic). Hence, $\mathbf{H}(s-s') = \mathbf{I}\mathrm{H}(\mathrm{s}-\mathrm{s}') = \mathbf{I}\left[\delta(s-s')/3\pi\eta + \Omega(s-s')\right]$, where $\gamma = 3\pi\eta$ has be used. For the latter, it is assumed that every segment is a sphere of diameter l with the friction coefficient $\hat{\gamma} = 3\pi\eta l$ (Stokes law). This leads to the friction density $\hat{\gamma}/l \to \gamma = 3\pi\eta$ in the continuum limit $l \to 0$.

Within the preaveraging approximation, the equation of motion (35) is linear and the eigenfunction expansion (19) leads to the equations of motion for the mode amplitudes

$$3\pi\eta\frac{\partial \boldsymbol{\chi}_k}{\partial t} = \sum_{n=0}^{\infty} \mathrm{H}_{kn}\left(-\frac{3\pi\eta}{\tau_n}\boldsymbol{\chi}_n + \boldsymbol{\Gamma}_n\right), \tag{38}$$

where $\mathrm{H}_{kn} = 3\pi\eta\Omega_{kn} + \delta_{kn}$ and

$$\Omega_{kn} = \frac{1}{\sqrt{6\pi^3}\eta} \int_0^L \int_0^L \varphi_k(s') \frac{1}{\sqrt{l|s-s'|}} \varphi_n(s) ds ds'. \tag{39}$$

The correlation functions of the random forces are given by

$$\langle \Gamma_{n\alpha}(t) \Gamma_{k\alpha'}(t') \rangle = 6\pi\eta k_B T \delta_{\alpha\alpha'} \delta(t-t') \mathrm{H}^{-1}_{nk}. \tag{40}$$

Eq. (38) is an infinite system of coupled linear differential equations, which can be solved (numerically) by diagonalization. For an analytical solution, the approximation

$$\Omega_{kn} \approx \sqrt{\frac{2}{3\pi^3}} \frac{\delta_{kn}}{\eta L} \int_0^L \frac{L-s}{\sqrt{ls}} \cos\left(\frac{n\pi s}{L}\right) ds \tag{41}$$

is used [14]. A numerical calculation confirms that the matrix Ω_{nk} is almost diagonal for the considered flexible polymers ($L/l \gg 1$). The equations of motion for the normal-mode amplitudes are then given by

$$\frac{\partial \boldsymbol{\chi}_n}{\partial t} = -\frac{\mathrm{H}_{nn}}{\tau_n} \boldsymbol{\chi}_n + \frac{\mathrm{H}_{nn}}{3\pi\eta} \boldsymbol{\Gamma}_n = -\frac{1}{\tilde{\tau}_n} \boldsymbol{\chi}_n + \frac{\mathrm{H}_{nn}}{3\pi\eta} \boldsymbol{\Gamma}_n, \tag{42}$$

with the relaxation times

$$\tilde{\tau}_n = \frac{\tau_n}{1 + 3\pi\eta\Omega_{nn}} \approx \frac{\eta}{\sqrt{3\pi} k_B T} \left(\frac{lL}{n}\right)^{3/2} \equiv \frac{\tau_Z}{n^{3/2}} \tag{43}$$

and the Zimm time $\tau_Z = \eta (lL)^{3/2} / (\sqrt{3\pi} k_B T)$ [14, 32]. The relaxation times τ_n are given in Eq. (21). Hydrodynamic interactions lead to a weaker dependence of the relaxation times on polymer length and mode number as the Rouse model. As for the non-hydrodynamic case, the normal-mode amplitudes are given by

$$\boldsymbol{\chi}_n(t) = \frac{\tau_n}{3\pi\eta\tilde{\tau}_n} \int_{-\infty}^{t} \exp\left(-\frac{t-t'}{\tilde{\tau}_n}\right) \boldsymbol{\Gamma}_n(t') dt', \tag{44}$$

and the correlation functions by

$$\langle \boldsymbol{\chi}_k(t) \boldsymbol{\chi}_n(0) \rangle = \frac{k_B T}{\pi\eta} \tau_n \delta_{kn} e^{-t/\tilde{\tau}_n} \ , \ \forall k, n \neq 0, \tag{45}$$

which include the relaxation times $\tilde{\tau}_n$. Hence, the correlation functions decay exponentially and are universal functions of $t/\tilde{\tau}_n$.

We performed mesoscale hydrodynamic simulations of a discrete Gaussian polymer model [33, 34]. In particular, we calculated the correlation functions of the normal-mode amplitudes. For a discrete model of N monomers, the amplitudes are given by $\boldsymbol{\chi}_n = \sum_{i=1}^{N} \boldsymbol{r}_i \cos(n\pi[i - 1/2]/N)$ and the non-draining relaxation times by $\tilde{\tau}_n \sim (n/N)^{1/2} / \sin^2(n\pi/N)$, which turn into $\tilde{\tau}_n \sim (L/n)^{3/2}$ [Eq. 43] in the continuum limit. Figure 4 displays autocorrelation functions for the mode amplitudes. Within the accuracy of the simulations, the correlation functions decay exponentially and exhibit the scaling behavior predicted by the Zimm model.

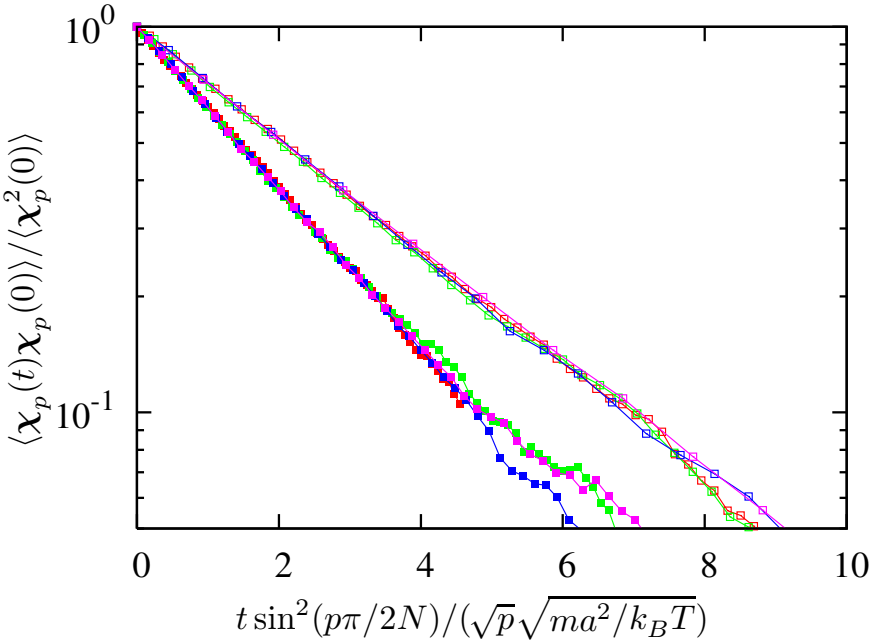

Fig. 4: *Correlation functions of the mode amplitudes of a non-draining Gaussian polymer for the modes* $p = 1 - 4$*. The polymer lengths are* $N = 20$ *(right) and* $N = 40$ *(left) [34].*

Experimentally, the normal-mode theory has been tested by measuring the fluctuations of single DNA molecules held in a partially extended state by optical tweezers [35]. The authors find that the motion of DNA can be described by linearly independent normal modes. However, they also found that the dependence of the relaxation times on the mode number is a function of the DNA extension a [23]. Figure 5 compares experimental data with theoretical results obtained by a semiflexible polymer model (see Eq. (8)) [23]. The analytical solution suggests that hydrodynamic interactions, the finite extensibility of the polymer, and its stiffness determine the observed relaxation time dependence. A free-draining, flexible polymer model does not describe the measured behavior.

(i) **Center-of-mass mean square displacement**

Equation (42) gives

$$\boldsymbol{\chi}_0(t) = \boldsymbol{\chi}_0(0) + \frac{\mathrm{H}_{00}}{3\pi\eta}\int_0^t \boldsymbol{\Gamma}_0(t')dt', \tag{46}$$

which yields the center-of-mass mean square displacement

$$\left\langle \Delta \boldsymbol{r}_{cm}(t)^2 \right\rangle = \frac{\mathrm{H}_{00}^2}{(3\pi\eta)^2}\int_0^t\int_0^t \langle \boldsymbol{\Gamma}_0(t')\boldsymbol{\Gamma}_0(t'')\rangle\, dt'dt'' = \frac{6k_BT}{3\pi\eta L}\mathrm{H}_{00}t, \tag{47}$$

and the diffusion coefficient ($L/l \gg 1$)

$$D_Z = \frac{k_BT}{3\pi\eta L}\mathrm{H}_{00} = \frac{8k_BT}{3\sqrt{6\pi^3}\eta}\frac{1}{\sqrt{lL}}. \tag{48}$$

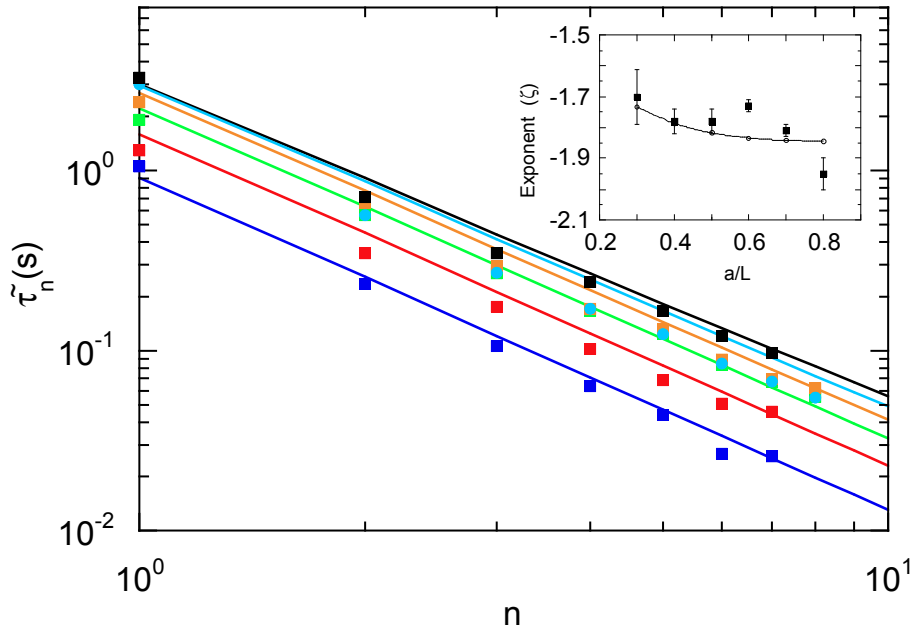

Fig. 5: *Relaxation times of DNA molecules for the extensions* $a/L = 0.3, 0.4, 0.5, 0.6, 0.7,$ *and* 0.8 *(top to bottom) [23]. The inset shows the exponents* ζ *of the relation* $\tilde{\tau}_n \sim n^\zeta$ *corresponding to the various curves. The experimental data (squares) are taken from Ref. [35].*

Evidently, diffusion in a dilute solution is faster than in a polymer melt at the same viscosity, as expressed by the ration $D_Z/D_R \sim \sqrt{L/l}$. The long-range hydrodynamic interactions enhance the diffusive dynamics by collective motion of the fluid.

Experimentally, the molecular weight dependence $D_Z \sim L^{-1/2}$ has been confirmed for polymers under Θ conditions, where excluded-volume interactions can be neglected, i.e., conditions under which the described model applies [14, 36–39]. However, the experimental value D_Z is about 15% smaller than the theoretical value (48) [14, 40]. Similar, computer simulations of polymers in solution yield the same molecular weight dependence and even D_Z is in close agreement with the theoretical prediction [34, 41, 42]. This displays the remarkable success of the Zimm model.

(ii) **Segmental mean square displacement**

Similar to the free-draining case, the averaged segmental mean square displacement is given by

$$\left\langle \Delta \boldsymbol{r}(t)^2 \right\rangle = 6D_Z t + \frac{2k_B T}{\pi \eta L} \sum_{n=1}^{\infty} \tau_n \left(1 - e^{-t/\tilde{\tau}_n}\right). \tag{49}$$

With the Zimm relaxation times (43), the sum is replaced by an integral as follows ($x_n = n(t/\tau_z)^{2/3}$)

$$\sum_{n=1}^{\infty} \frac{\tau_R}{n^2} \left[1 - e^{-tn^{3/2}/\tau_z}\right] \to \left(\frac{t}{\tau_z}\right)^{2/3} \tau_R \int_0^\infty \frac{1}{x^2} \left[1 - e^{-x^{3/2}}\right] dx. \tag{50}$$

Hence, $\langle \Delta \boldsymbol{r}^2 \rangle \sim t^{2/3}$, i.e., hydrodynamic interactions lead to a stronger time dependence of the segmental MSD compared to the free-draining case.

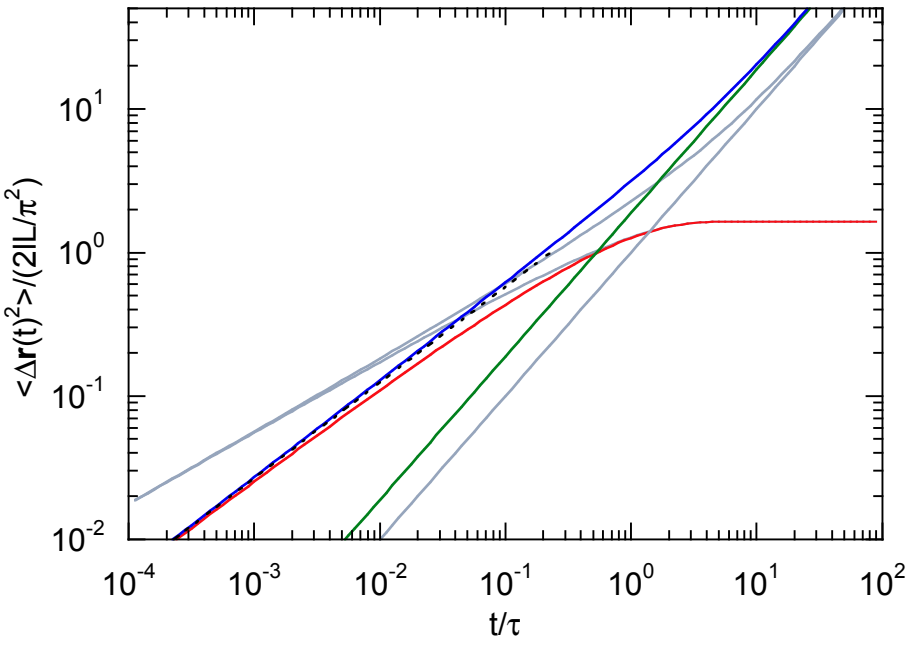

Fig. 6: *Mean square displacements of polymers in dilute solution. The gray lines correspond to the Rouse model (see Fig. 3) and the colored lines to the non-draining Zimm model. The green line indicates* $\langle \Delta \boldsymbol{r}_{cm}(t)^2 \rangle$*, the blue line the total MSD* $\langle \Delta \boldsymbol{r}(t)^2 \rangle$*, and the red line the segmental MSD in the center-of-mass reference frame* $\langle \Delta \boldsymbol{r}(t)^2 \rangle - \langle \Delta \boldsymbol{r}_{cm}(t)^2 \rangle$*. The red line approaches the asymptotic value* $2R_G^2$ *in the limit* $t \to \infty$*. The dotted line represents the analytical approximation (50), where the integral is* 2.6789*.*

The center-of-mass (47) and segmental (49) MSDs are displayed in Fig. 6. As for the Rouse model, for $t/\tau_Z \ll 1$, the total MSD is dominated by the internal dynamics, i.e., the second term in Eq. (47). Here, the full numerical result and the analytical approximation closely agree with each other, and the MSD increase as $t^{2/3}$. For $t/\tau_R \gg 1$, the MSD is given by the center-of-mass displacement. The deviation between the analytical and numerical solutions in the regime $5 \times 10^{-3} < t/\tau_Z < 10^{-1}$ shows that the $t^{2/3}$ behavior can only be observed for very long polymers and hence a large number of normal modes.

Fluorescence correlation spectroscopy (FCS), a single-molecule technique, provides detailed information on dynamical properties of individual macromolecules [25,30,43]. In Ref. [25], the diffusion and segmental dynamics has been studied of single-end fluorescently labeled dsDNA fragments in the length range from 10^2 to 2×10^4 base pairs (bp), corresponding to $L/l_p \approx 0.7 - 140$. From the correlation function, the mean square displacement of the labeled end is easily extracted. Figure 7 shows the experimental results together with the predictions of the non-draining Gaussian semiflexible polymer model [26, 27, 30, 44]. The theoretical curves are in excellent agreement with the experimental data. To achieve the agreement, an adjustment of the time scale of the model with the diagonal Oseen tensor (41) is necessary. We replaced Ω_{nn} by $\Lambda\Omega_{nn}$ and Ω_{00} by $\Lambda_D\Omega_{00}$, with $\Lambda = 0.6$ and $\Lambda_D = 0.9$ [25]. As shown in Ref. [45], agreement without fit parameter can be achieved, when the full tensor Ω_{nm} is taken into account. Moreover, Brownian dynamics simulations underline the success of the semiflexible polymer model [45, 46]. For short DNA fragments, the polymer dynamics is dominated by the center-

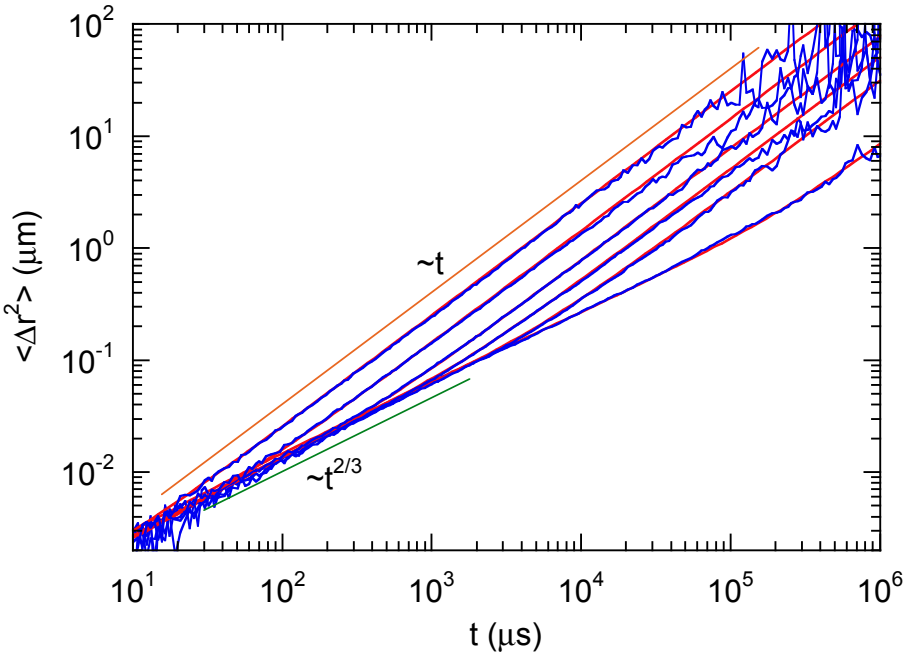

Fig. 7: *Mean square displacements of an end segment of dsDNA molecules of lengths* $L/\mathrm{bp} = 100,\ 200,\ 500,\ 1000,\ 2000,\ 2000$ *(top to bottom). The blue lines are experimental results from Ref. [25], and the red lines are calculated by the semiflexible Gaussian polymer model.*

of-mass motion of the whole molecule in the considered time window. For longer molecules, also the internal dynamics (50) is experimentally accessible. Here, the slope of the MSD is close to $t^{2/3}$ as predicted by theory. The experimental and simulation studies demonstrate that DNA molecules can be considered as semiflexible polymers with their dynamics controlled by hydrodynamic interactions.

The success of the non-draining Gaussian semiflexible polymer model is not a priori evident—the calculations involve a number of approximations, such as the preaveraging approximation. Brownian dynamics simulations reproduce the free-draining behavior less accurately, which suggests that the long-range hydrodynamic interactions contribute to the success of the mean-field model [45].

3.3 Excluded-Volume Interactions

So far, polymers in a Θ solvent have been discussed, i.e., polymers, where the excluded-volume interactions between the various monomers are screened. Experimentally, it has been show that this is an adequate description of polymers in melts (see contribution E 3). In dilute solution under so-called good solvent conditions, excluded-volume interactions lead to a swelling of a polymer coil. The mean square end-to-end distance increases then with the power law $\langle(\boldsymbol{r}_N - \boldsymbol{r}_0)^2\rangle \sim l^2 N^{2\nu}$ with polymer length, where mean field approaches predict $\nu = 0.6$ and more precise renormalization group calculations $\nu \approx 0.588$ [11, 14]. The swelling also affects the dynamics of a polymer. Qualitatively, this effect can be captured by the linearization approximation [14]. Here the distribution function $\Psi(\boldsymbol{r}(s) - \boldsymbol{r}(s')) = F(|\boldsymbol{r}(s) - \boldsymbol{r}(s')|/[|(s-s')/l|^\nu])$

is used, which gives

$$\left\langle \frac{1}{|\boldsymbol{r}(s)-\boldsymbol{r}(s')|} \right\rangle \approx \left(\frac{l}{|s-s'|} \right)^{\nu} \tag{51}$$

and leads to the relaxation times $(L/l \gg 1)$ [14]

$$\tilde{\tau}_n \approx \frac{\eta l^3}{k_B T} \left(\frac{L}{ln} \right)^{3\nu}. \tag{52}$$

With the exponent $\nu = 1/2$ for a Θ solvent, the dependencies (43) are recovered. Renormalization group theory calculations yield the diffusion coefficient $D_Z = 0.2 k_B T/(\sqrt{6}\eta R_G)$ in good solvent, with the radius of gyration $R_G \approx l(L/l)^{\nu}$ [14, 47].

4 Dynamic Structure Factor

The dynamical properties of polymers can be studied by scattering experiments such as dynamic light scattering [48] or neutron scattering (see lecture E 3). Here, the dynamic structure factor

$$S(\boldsymbol{q},t) = \frac{1}{L^2} \int_0^L \int_0^L \langle \exp\left(i\boldsymbol{q}[\boldsymbol{r}(s,t)-\boldsymbol{r}(s',0)]\right)\rangle \, ds ds' \tag{53}$$

is obtained [14]. For the considered polymer model, the average can easily be evaluated, because of the linearity of the model and the Gaussian nature of the underlying stochastic process. Hence, $S(\boldsymbol{q},t)$ becomes

$$S(\boldsymbol{q},t) = \frac{1}{L^2} \int_0^L \int_0^L \exp\left(-\frac{1}{6}\boldsymbol{q}^2 \left\langle [\boldsymbol{r}(s,t)-\boldsymbol{r}(s',0)]^2 \right\rangle \right) ds ds'. \tag{54}$$

With the eigenfunction expansion (19), the exponent can be written as

$$\left\langle [\boldsymbol{r}(s,t)-\boldsymbol{r}(s',0)]^2 \right\rangle = \sum_{n=0}^{\infty} \left[\left\langle \boldsymbol{\chi}_n^2 \right\rangle \left(\varphi_n(s)^2 + \varphi_n(s')^2 \right) - 2 \left\langle \boldsymbol{\chi}_n(t)\boldsymbol{\chi}_n(0) \right\rangle \varphi_n(s)\varphi_n(s') \right]. \tag{55}$$

Equation (54) can be simplified exploiting the equilibrium expression

$$\left\langle [\boldsymbol{r}(s,0)-\boldsymbol{r}(s',0)]^2 \right\rangle = \sigma^2(s,s') = \sum_{n=0}^{\infty} \left\langle \boldsymbol{\chi}_n^2 \right\rangle [\varphi_n(s)-\varphi_n(s')]^2 \tag{56}$$

and the corresponding static structure factor

$$S(\boldsymbol{q},0) = \frac{1}{L^2} \int_0^L \int_0^L \exp\left(-\frac{\boldsymbol{q}^2}{6}\sigma^2(s,s') \right) ds ds', \tag{57}$$

which yields

$$S(\boldsymbol{q},t) = \frac{e^{-\boldsymbol{q}^2 Dt}}{L^2} \int_0^L \int_0^L \exp\left(-\frac{\boldsymbol{q}^2}{6} l|s-s'| \right) \times \exp\left(-\frac{\boldsymbol{q}^2 k_B T}{3\pi\eta} \sum_{n=1}^{\infty} \tau_n \varphi_n(s)\varphi_n(s')(1-e^{t/\hat{\tau}_n}) \right) ds ds'. \tag{58}$$

Here, D and $\hat{\tau}_n$ are either the Rouse or Zimm diffusion coefficient and relaxation times, depending on the underlying model. The last term in Eq. (58) describes the internal dynamics of the polymer in the center-of-mass reference frame.

(i) **Small angle regime**: $\boldsymbol{q}^2 lL \ll 1$

For $\boldsymbol{q}^2 lL \ll 1$, the exponents of the terms under the integrals are much smaller than unity and the integrals are well approximated by L^2 (see Fig. 6). Hence,

$$S(\boldsymbol{q},t) = e^{-\boldsymbol{q}^2 Dt}, \tag{59}$$

i.e., the diffusive motion of a polymer coil is measured [14, 20].

(ii) **Large angle regime**: $\boldsymbol{q}^2 lL \gg 1$

To study the internal dynamics of a polymer, the regime $\boldsymbol{q}^2 lL \gg 1$ has to be considered, i.e., the wave length of the scattering vector has to be significantly smaller than the polymer root mean square end-to-end distance. It is sufficient to consider the time regime $t/\hat{\tau}_1 \ll 1$, because $S(\boldsymbol{q},t)$ is very small for $t/\hat{\tau}_1 \gg 1$ [14]. Moreover, the contribution of the translation motion can be neglected, since Dt is much smaller than the contribution from the internal dynamics (see Figs. 3, 6). The integrand in Eq. (58) has a sharp peak at $s = s'$ for the considered large scattering vectors, which yields the expression [20]

$$S(\boldsymbol{q},t) = \frac{2}{L}\int_0^L \exp\left(-\frac{\boldsymbol{q}^2}{6} ls\right) \exp\left(-\frac{\boldsymbol{q}^2 k_B T}{3\pi\eta L}\sum_{n=1}^{\infty} \tau_n \cos\left(\frac{n\pi s}{L}\right)\left(1 - e^{t/\hat{\tau}_n}\right)\right) ds. \tag{60}$$

As for the mean square displacement, the discrete sum can be replaced by an integral.

4.1 Rouse Model

In the integral representation, for the Rouse model follows

$$S(\boldsymbol{q},t) = \frac{12}{q^2 lL}\int_0^{q^2 lL/6} \exp\left(-u - (\Gamma_R(q)t)^{1/2} h\left(u[\Gamma_R(q)t]^{-1/2}\right)\right) du, \tag{61}$$

where ($\gamma = 3\pi\eta$)

$$\Gamma_R(q) = \frac{q^4 l k_B T}{36\pi\eta} \tag{62}$$

and

$$h(u) = \frac{2}{\pi}\int_0^{\infty} \frac{\cos(xu)}{x^2}(1 - e^{-x^2})dx. \tag{63}$$

For $\Gamma_R(q)t \gg 1$, the cosine can be replaced by unity which leads to [14]

$$S(\boldsymbol{q},t) = S(\boldsymbol{q},0)\exp\left(-\frac{2}{\sqrt{\pi}}\left[\Gamma_R(q)t\right]^{1/2}\right). \tag{64}$$

Hence, $S(\boldsymbol{q},t)$ is a universal function of $\Gamma_R t \sim q^4 t$.

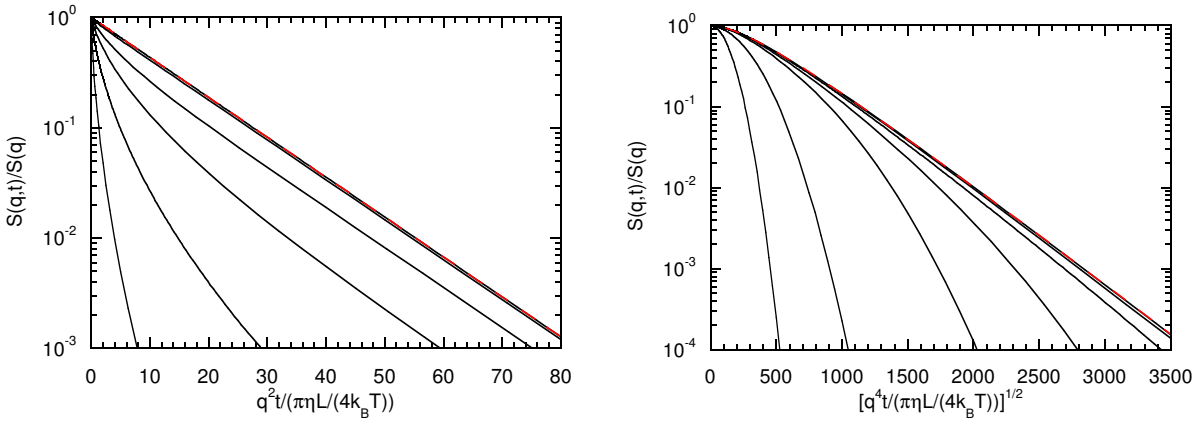

Fig. 8: *Normalized dynamic structure factors of the Rouse model for $L/l = 10^3$ and various q values. The black lines correspond to the full solution of Eq. (58). Left: $S(\boldsymbol{q},t)$ as function of q^2t for $qL = 1$, 100, 200, 300, 500, and 1000 (right to left). Right: $S(\boldsymbol{q},t)$ as function of q^4t for $qL = 50$, 100, 200, 300, 500, 1000, and 3000 (left to right). Note, $q^2lL = 1$ for $qL\sqrt{10^3}$. The red dashed lines indicate the limit (59) for $q^2lL \ll 1$ (left) and (61) for $q^2lL \gg 1$ (right).*

Figure 8 shows dynamic structure factors for $L/l = 10^3$. Hence, for $qL = \sqrt{10^3}$ is $q^2lL = 1$. Then, the conditions $q^2lL \ll 1$ and $q^2lL \gg 1$ translate to $qL \ll 30$ and $qL \gg 30$, respectively. The left figures shows that a universal behavior is obtained for $pL < 30$, where $S(\boldsymbol{q},t)$ is a function of q^2t only. The red dashed line shows the dependence $S(q,t)/S(q,0) = e^{-q^2Dt}$, i.e., the dynamic structure factor decays exponentially in this limit. In the limit $qL \gg 30$, $S(q,t)$ is a universal function of q^4t. As indicated in Fig. 8 (right), the theoretically predicted limit (61) (red dashed line) is assumed for large enough qL-values—in the current case for $qL \gtrsim 10^3$. $S(q,t)$ exhibits the predicted exponential decay (64) for $[q^4t/(\eta L/k_BT)]^{1/2} \gg 1$ only.

4.2 Zimm Model

Similar to the continuum limit (50), the structure factor in the presence of hydrodynamic interactions becomes ($x_n = n(\sqrt{2}t/\tau_Z)^{2/3}$)

$$S(\boldsymbol{q},t) = \frac{12}{q^2lL}\int_0^{q^2lL/6} \exp\left(-u - (\Gamma_Z(q)t)^{2/3}h\left(u[\Gamma_Z(q)t]^{-2/3}\right)\right) du, \tag{65}$$

where

$$\Gamma_Z(q) = \frac{q^3k_BT}{6\pi\eta} \tag{66}$$

and

$$h(u) = \frac{2}{\pi}\int_0^\infty \frac{\cos(xu)}{x^2}(1 - e^{-x^{3/2}/\sqrt{2}})dx. \tag{67}$$

For $\Gamma_Z(q)t \gg 1$ follows [14]

$$S(\boldsymbol{q},t) = S(\boldsymbol{q},0)\exp\left(-1.35\left[\Gamma_Z(q)t\right]^{2/3}\right). \tag{68}$$

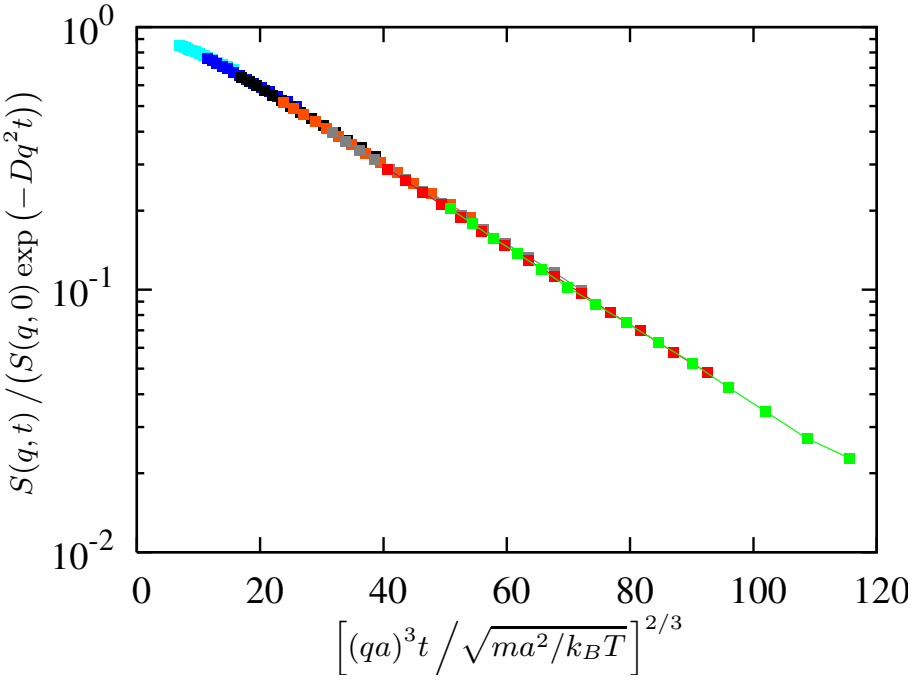

Fig. 9: *Normalized dynamic structure factor of a polymer of length $N = 40$ in dilute solution with excluded volume interactions and for various q values [34].*

Here, $S(\boldsymbol{q}, t)$ is a universal function of $\Gamma_Z t \sim q^3 t$.

There is a clear difference in the dynamic structure factor of the free-draining and non-draining case, which allows us to assess the relevance of hydrodynamic interactions both, experimentally and by simulations.

Our mesoscale hydrodynamic simulations [34] yield the dynamic structure factor displayed in Fig. 9. Independent of the solvent conditions (Θ or good solvent), the Zimm model predicts the scaling relation $S(\boldsymbol{q}, t) = S(\boldsymbol{q}, 0) f(q^3 t)$. Evidently, the simulation results are in agreement with the theoretical prediction, although the function does not decay exponentially at short times. This is similar to $S(\boldsymbol{q}, t)$ of Fig. 8 (right).

5 Conclusions

Naturally, the dynamics of polymers in solution and melt cannot be presented in a comprehensive way in this lecture note. Here, only certain basic aspects have been touched and outlined. There would be much more to be discussed for semiflexible polymers as well as long polymers in melts. In the latter case, the non-crossability of the polymers leads to entanglements and a tube-like confined of a particular polymer by its neighborhood [14] and gives rise to additional power-law regimes in the diffusive dynamics [11, 14].

Appendices

A Oseen Tensor

The Stokes equation of the fluid flow field $\boldsymbol{v}(\boldsymbol{r})$ is given by [19]

$$\eta\Delta\boldsymbol{v} = \nabla p - \boldsymbol{f}, \tag{69}$$

where η is the fluid viscosity, p the pressure, and $\boldsymbol{f}$ an external volume force. The linear equation can be solved by Fourier transformation

$$\boldsymbol{v}_k = \int \boldsymbol{v}(\boldsymbol{r}) e^{i\boldsymbol{k}\boldsymbol{r}} d^3r, \tag{70}$$

which yields

$$\eta\boldsymbol{k}^2\boldsymbol{v}_k + i\boldsymbol{k}p_k = \boldsymbol{f}_k. \tag{71}$$

For an incompressible fluid, where $\nabla\boldsymbol{v} = 0$, follows $\boldsymbol{k}\boldsymbol{v}_k = 0$, i.e., $\boldsymbol{v}_k \perp \boldsymbol{k}$. Multiplication of Eq. (71) with $\boldsymbol{k}$, allows one to eliminate p_k and to obtain the closed expression

$$\boldsymbol{v}_k = \frac{1}{\eta\boldsymbol{k}^2}\left(\mathbf{I} - \frac{\boldsymbol{k}:\boldsymbol{k}}{\boldsymbol{k}^2}\right)\boldsymbol{f}_k,$$

where $\boldsymbol{k}:\boldsymbol{k}$ denotes the tensor product. Fourier transformation gives

$$\boldsymbol{v}(\boldsymbol{r}) = \int \boldsymbol{\Omega}(\boldsymbol{r}-\boldsymbol{r}')\boldsymbol{f}(\boldsymbol{r}')d^3r', \tag{72}$$

with

$$\boldsymbol{\Omega}(\boldsymbol{r}) = \frac{1}{(2\pi)^3}\int \frac{1}{\eta\boldsymbol{k}^2}\left(\mathbf{I} - \frac{\boldsymbol{k}:\boldsymbol{k}}{\boldsymbol{k}^2}\right)e^{-i\boldsymbol{k}\boldsymbol{r}}d^3k,$$

which yields the *Oseen* tensor [14, 19]

$$\boldsymbol{\Omega}(\boldsymbol{r}) = \frac{1}{8\pi\eta r}\left(\mathbf{I} + \frac{\boldsymbol{r}:\boldsymbol{r}}{r^2}\right). \tag{73}$$

References

[1] L. Eichinger, B. Köppel, A. Noegle, M. Schleicher, M. Schliwa, K. Weijer, W. Witke, and P. Janmey, Biophys. J. **70**, 1054 (1996).

[2] P. Janmey, in *Handbook of Biological Physics* (North Holland, Amsterdam, 1995), vol. 1A, chap. 17.

[3] T. L. Hill, *Statistical Mechanics* (MCGraw-Hill, New York, 1956).

[4] H. B. Callen, *Thermodynamics* (Wiley, New York, 1961).

[5] A. Münster, *Statistical Thermodynamics*, vol. I (Springer, Berlin, 1969).

[6] D. Ruelle, *Statistical Mechanics* (W. A. Benjamin, New York, 1969).

[7] D. Chandler, *Introduction to Modern Statistical Mechanics* (Oxford University Press, Oxford, 1987).

[8] P. Reineker, M. Schulz, and B. M. Schulz, *Theoretische Physik V* (Wiley-VCH, Weinheim, 2010).

[9] M. V. Volkenstein, *Configurational Statistics of Polymer Chains* (Interscience, New York, 1963).

[10] L. R. G. Treloar, *The Physics of Rubber Elasticity* (Clarendon Press, Oxford, 1975).

[11] P.-G. de Gennes, *Scaling Concepts in Polymer Physics* (Cornell University, Ithaca, 1979).

[12] J. H. Weiner, *Statistical Mechanics of Elasticity* (Wiley, New York, 1983).

[13] P. J. Flory, *Statistical Mechanics of Polymer Chains* (John Wiley & Sons, New York, 1989).

[14] M. Doi and S. F. Edwards, *The Theory of Polymer Dynamics* (Clarendon Press, Oxford, 1986).

[15] H. Kleinert, *Path Integrals in Quantum Mechanics, Statistics, and Polymer Physics* (World Scientific, Singapore, 1990).

[16] R. G. Winkler, P. Reineker, and L. Harnau, J. Chem. Phys. **101**, 8119 (1994).

[17] H. Risken, *The Fokker-Planck Equation* (Springer, Berlin, 1989).

[18] H. C. Öttinger, *Stochastic Processes in Polymeric Fluids* (Springer, Berlin, 1996).

[19] J. K. G. Dhont, *An Introduction to Dynamics of Colloids* (Elsevier, Amsterdam, 1996).

[20] L. Harnau, R. G. Winkler, and P. Reineker, J. Chem. Phys. **104**, 6355 (1996).

[21] P.-G. de Gennes, J. Chem. Phys. **55**, 572 (1971).

[22] T. C. B. McLeish, Adv. Phys. **51**, 1379 (2002).

[23] R. G. Winkler, Phys. Rev. Lett. **82**, 1843 (1999).

[24] R. G. Winkler, J. Chem. Phys. **118**, 2919 (2003).

[25] E. P. Petrov, T. Ohrt, R. G. Winkler, and P. Schwille, Phys. Rev. Lett. **97**, 258101 (2006).

[26] R. G. Winkler, J. Chem. Phys. **133**, 164905 (2010).

[27] R. G. Winkler, Phys. Rev. Lett. **97**, 128301 (2006).

[28] R. G. Winkler, Soft Matter **6**, 6183 (2010).

[29] O. Kratky and G. Porod, Recl. Trav. Chim. Pays-Bas **68**, 1106 (1949).

[30] R. G. Winkler, S. Keller, and J. O. Rädler, Phys. Rev. E **73**, 041919 (2006).

[31] P. E. Rouse, J. Chem. Phys. **21**, 1272 (1953).

[32] B. H. Zimm, J. Chem. Phys. **24**, 269 (1956).

[33] M. Ripoll, K. Mussawisade, R. G. Winkler, and G. Gompper, Europhys. Lett. **68**, 106 (2004).

[34] K. Mussawisade, M. Ripoll, R. G. Winkler, and G. Gompper, J. Chem. Phys. **123**, 144905 (2005).

[35] S. R. Quake, H. Babcock, and S. Chu, Nature **388**, 151 (1997).

[36] T. A. King, A. Knox, W. I. Lee, and J. D. G. McAdam, Polymer **14**, 151 (1973).

[37] M. Adam and M. Delsanti, Macromolecules **10**, 1229 (1977).

[38] T. Nose and B. Chu, Macromolecules **12**, 590 (1979).

[39] C. C. Han and A. Z. Akcasu, Macromolecules **14**, 1080 (1981).

[40] W. H. Stockmayer and B. Hammouda, Pure & Appl. Chem. **56**, 1373 (1984).

[41] M. Fixman, J. Chem. Phys. **78**, 1594 (1983).

[42] B. Liu and B. Dünweg, J. Chem. Phys. **118**, 8061 (2003).

[43] E. P. Petrov and P. Schwille, in *Standardization and Quality Assurance in Fluorescence Measurements II*, edited by U. Resch-Genger (Springer Berlin Heidelberg, 2008), vol. 6 of *Springer Series on Fluorescence*, p. 145.

[44] R. G. Winkler, J. Chem. Phys. **127**, 054904 (2007).

[45] M. Hinczewski and R. Netz, EPL **88**, 18001 (2009).

[46] M. Hinczewski, X. Schlagberger, M. Rubinstein, O. Krichevsky, and R. R. Netz, Macromolecules **42**, 860 (2009).

[47] Y. Oono and M. Kohmoto, J. Chem. Phys. **78**, 520 (1983).

[48] B. J. Berne and R. Pecora, *Dynamic Light Scattering* (Wiley, New York, 1976).